PAPER

Passive on-chip isolators based on the thin-film lithium niobate platform

To cite this article: Jiacheng Liu *et al* 2025 *Chinese Phys. B* **34** 034204

Passive on-chip isolators based on the thin-film lithium niobate platform

Jiacheng Liu(刘嘉成)[1], Gongyu Xia(夏功榆)[1], Qilin Hong(洪琦琳)[1], Pingyu Zhu(朱枰谕)[2], Kai-Kai Zhang(张凯凯)[2], Keyu Xia(夏可宇)[3], Ping Xu(徐平)[2], Shiqiao Qin(秦石乔)[1], and Zhihong Zhu (朱志宏)[1,†]

[1] *College of Advanced Interdisciplinary Studies & Hunan Provincial Key Laboratory of Novel Nano Optoelectronic Information Materials and Devices, National University of Defense Technology, Changsha* 410073, *China*

[2] *Institute for Quantum Information and State Key Laboratory of High-Performance Computing, College of Computer Science and Technology, National University of Defense Technology, Changsha* 410073, *China*

[3] *College of Engineering and Applied Sciences, National Laboratory of Solid State Microstructures, and Collaborative Innovation Center of Advanced Microstructures, Nanjing University, Nanjing* 210023, *China*

(Received 17 September 2024; revised manuscript received 12 December 2024; accepted manuscript online 24 December 2024)

Optical isolators, the photonic analogs of electronic diodes, are essential for ensuring the unidirectional flow of light in optical systems, thereby mitigating the destabilizing effects of back reflections. Thin-film lithium niobate (TFLN), hailed as "the silicon of photonics," has emerged as a pivotal material in the realm of chip-scale nonlinear optics, propelling the demand for compact optical isolators. We report a breakthrough in the development of a fully passive, integrated optical isolator on the TFLN platform, leveraging the Kerr effect to achieve an impressive 10.3 dB of isolation with a minimal insertion loss of 1.87 dB. Further theoretical simulations have demonstrated that our design, when applied to a microring resonator with a Q factor of 5×10^6, can achieve 20 dB of isolation with an input power of merely 8 mW. This advancement underscores the immense potential of lithium niobate-based Kerr-effect isolators in propelling the integration and application of high-performance on-chip lasers, heralding a new era in integrated photonics.

Keywords: thin-film lithium niobate, Kerr effect, optical isolator

PACS: 42.82.–m, 42.82.Et, 42.65.Hw

DOI: 10.1088/1674-1056/ada2ef **CSTR:** 32038.14.CPB.ada2ef

1. Introduction

Advanced nanofabrication technology has enabled dramatic advances in integrated photonics platforms. The advantages of compact size, light weight, and low power consumption of integrated photonics platforms have greatly facilitated the development of optical communications,[1,2] microwave photonics,[3] computing,[4,5] optical atomic clocks,[6] quantum information processing,[7–9] optical ranging,[10–12] and sensing.[13–15] Through heterogeneous integration technology, on-chip lasers[16] have been able to be efficiently integrated with ultra-low-loss passive optical chips. Light emission, nonlinearity, and detection on a single chip have become possible. However, there is an urgent need for a high-performance and reliable integrated optical isolator for narrow linewidth semiconductor lasers combined with functional photonic modules.

Optical isolators serve as non-reciprocal devices that facilitate the unidirectional transmission of light, playing a pivotal role in optical systems by preventing back-reflected light from interfering with the laser source, thereby reducing noise and stabilizing laser power. The realization of on-chip optical isolators can be achieved through various mechanisms, including magneto–optical effects,[17–21] electro–optical effects,[22–29] acousto–optical interactions,[30–32] and nonlinear optical phenomena.[33–36] The Faraday effect capitalizes on the non-reciprocal transmission of light in magneto–optical crystals subjected to an external magnetic field, leveraging the polarization rotation induced by the Faraday effect. Magneto–optical crystals, long utilized in traditional optical fibers and bulk optics as isolators, have been successfully integrated into waveguides. Nonetheless, the integration of magneto–optical crystals in optical chips necessitates external magnetic fields for isolation, demanding stringent control over these magnetic fields to avert interference from extraneous magnetic influences.[37] Furthermore, the fabrication of magneto–optical crystals is not compatible with complementary metal–oxide–semiconductor (CMOS) processes, a limitation that hinders the broader development of this technology.

The quest for alternative approaches has led to significant strides in the development of active magnet-free isolators leveraging electro–optic and acousto–optic effects. These isolators achieve unidirectional light propagation through differential phase modulation of forward and backward light, offering the benefits of high isolation ratios and expansive tuning bandwidths. However, the reliance on external drivers for ac-

[†]Corresponding author. E-mail: zzhwcx@163.com

tive magnet-free isolators introduces additional complexities. The integration of structures such as electrodes on-chip elevates the fabrication intricacy. The necessity for an external power supply to energize these drivers escalates power consumption. Moreover, the complex electromagnetic fields engendered by high-power radio-frequency (RF) drives can perturb on-chip photodetection and other precision devices, introducing potential sources of noise and interference. These multifaceted challenges underscore the need for innovative solutions in the evolution of photonic chips. The ideal isolator for integrated photonics must embody a completely passive and magnet-free design, devoid of the need for external drivers or power sources. Such a device would not only mitigate the complexity of fabrication but also minimize power consumption and the risk of electromagnetic interference, thereby facilitating the seamless integration with other photonic components and the advancement of high-performance, reliable, and scalable photonic systems.

Nonlinearity stands as an intrinsic attribute of a spectrum of material platforms that underpin the field of integrated photonics. This property is notably present in silicon,[38] silicon nitride,[39] silicon carbide,[40] and gallium phosphide,[41] enabling a myriad of applications across nonlinear optics. The successful demonstration of optical isolators that harness nonlinear effects, as seen in silicon nitride microring resonators[33] and silica microrod resonators,[34] has illuminated the virtues of passive operation and structural simplicity. In recent years, thin-film lithium niobate (TFLN) has emerged as a compelling integrated photonics platform. TFLN's expansive transparency window, coupled with its substantial second-order nonlinearities and significant piezoelectric coefficients, positions it as an attractive candidate for the development of future coherent optical systems. Its third-order nonlinear coefficient of 1.6×10^{-21} $\mathrm{m^2/V^2}$[42] is on par with that of silicon nitride, a material widely favored for third-order nonlinear applications. Given these attributes, the TFLN platform is particularly well-suited for the creation of a new generation of photonic devices that can perform sophisticated manipulations of light, such as frequency conversion and optical parametric processes. Besides, TFLN is regarded as the most promising platform for achieving high-performance integrated electro–optic modulators due to its excellent electro–optic characteristics.[43] These advantages are propelling the integration of lasers with the TFLN platform. To achieve this goal, a crucial prerequisite is the availability of a stable and reliable passive optical isolator to prevent spurious reflections from entering the laser cavity. Such an isolator would not only significantly enhance the performance of systems based on TFLN but also meet the need for devices that can operate without dependence on external power sources or magnetic fields.

Here, we unveil a groundbreaking and elegantly simple design for integrated continuous-wave optical isolators, capitalizing on the Kerr effect exhibited in microring resonators fabricated from TFLN. The Kerr effect orchestrates a spontaneous symmetry-breaking phenomenon for the circulating modes within the microring, distinguishing between clockwise and counterclockwise propagation and thereby enabling nonreciprocal light transmission.[33] Our optical isolator design eschews the need for complex external drivers, relying instead on the inherent properties of the microring resonator alone. This results in an optical isolator with an impressive isolation of up to 10.3 dB, coupled with a minimal insertion loss of merely 1.87 dB. The device is replete with advantages such as a streamlined structure, inherent passivity, and a remarkably low power footprint. The demonstration of this isolator not only simplifies the integration process but also addresses the persistent challenge of power consumption in conventional designs. The high level of isolation achieved, without the reliance on external magnetic fields or electrical driving, is a testament to the potential of TFLN as a material platform for creating passive and efficient photonic devices.

2. Basic theory

The Kerr effect encapsulates the phenomenon where the refractive index of a material undergoes a change in response to an applied electric field, a manifestation of nonlinear optics. When subjected to the influence of two electric fields, the nonlinear polarization that arises from this interaction is expressed by the equation $P^{(3)}(t)=\varepsilon_0\chi^{(3)}(E_1\,\mathrm{e}^{-\mathrm{i}\omega_1 t}+E_2\,\mathrm{e}^{-\mathrm{i}\omega_2 t}+\mathrm{c.c.})^3$, where ε_0 is the vacuum permittivity, $\chi^{(3)}$ is the third-order nonlinear susceptibility, and $E_{1,2}$ are the amplitudes of the electric fields at frequencies ω_1 and ω_2, respectively. Upon expansion of this polynomial and retention of only the terms that are resonant with the frequencies of interest, we can identify the specific contributions to the nonlinear polarization that are relevant to our analysis.

$$\begin{aligned} P^{(3)}(\omega_1)&=3\varepsilon_0\chi^{(3)}(|E_1|^2+2\,|E_2|^2)E_1\,\mathrm{e}^{-\mathrm{i}\omega_1 t},\\ P^{(3)}(\omega_2)&=3\varepsilon_0\chi^{(3)}(2\,|E_1|^2+|E_2|^2)E_2\,\mathrm{e}^{-\mathrm{i}\omega_2 t}. \end{aligned} \tag{1}$$

From Eq. (1), we can see that light intensity linearly affects the refractive index of the material itself. The two electric fields have different effects on their own refractive index and other refractive index, and these two effects are self-phase modulation (SPM) and cross-phase modulation (XPM). SPM is a nonlinear phase modulation under the action of its own intensity, while XPM is the nonlinear phase modulation under the action of the other light's intensity. In third-order nonlinear materials, the refractive index change induced by SPM and XPM for two counter-propagating light waves can be expressed as[43]

$$\Delta n_{\mathrm{a}}=\frac{n_2(P_{\mathrm{a}}+2P_{\mathrm{b}})}{A_{\mathrm{eff}}},$$

$$\Delta n_{\mathrm{b}} = \frac{n_2(P_{\mathrm{b}} + 2P_{\mathrm{a}})}{A_{\mathrm{eff}}} \tag{2}$$

with subscripts a and b indicating the two counter-propagating light waves with powers $P_{\mathrm{a,b}}$. n_2 is the nonlinear refractive index and A_{eff} is the effective mode cross-section. We can clearly see that the refractive index change caused by XPM is twice that of SPM. For two counter-propagating waves with a significant difference in power ($P_{\mathrm{a}} \gg P_{\mathrm{b}}$), the high-power forward-transmitting light will only receive the phase change caused by SPM, and the phase change caused by XPM is negligible. The weak-power backward-transmitting light is mainly receiving the phase change caused by XPM.

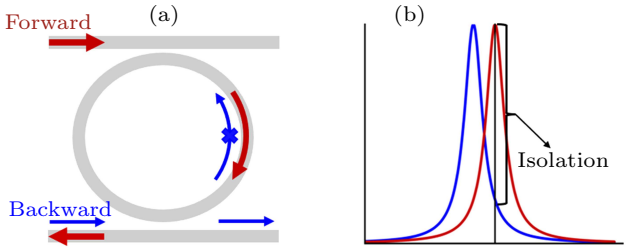

Fig. 1. (a) Non-reciprocal principle for micro-ring resonators. The forward light passes through the ring and exits from the drop port, while the backward light exits from the through port due to splitting of the resonant modes. (b) Mode splitting due to the Kerr effect, where red indicates the mode of forward transmission and blue the mode of backward transmission.

We harness this principle to craft an optical isolator within a TFLN add-drop microring resonator, as depicted in Fig. 1(a). The microring resonators possess degenerate clockwise (CW) and counterclockwise (CCW) modes. Upon the introduction of a high-power pump light into the microring resonator, the resonance frequencies of the CW and CCW modes experience a splitting attributed to SPM and XPM, as illustrated in Fig. 1(b). The resonance shift instigated by XPM is observed to be twice that caused by SPM. With the presence of a strong forward pump and a weak backward signal propagating along the ring, the existing resonant modes facilitate near-perfect transmission in the forward direction while significantly attenuating the transmission at the equivalent frequency in the backward direction. We denote the isolation arising from this phenomenon in Fig. 1(b). Adhering to the methodology outlined in Ref. [33], we derive the anticipated level of isolation

$$I = \frac{1}{1 + \left(2Q\dfrac{\Delta\omega}{\omega_0}\right)^2} \tag{3}$$

and the shift $\Delta\omega$ is given by

$$\Delta\omega = \omega_0 \frac{n_2}{n} \frac{Q\lambda}{2\pi V} \eta P_{\mathrm{in}}, \tag{4}$$

where Q is the loaded quality factor of the microring resonator, n is the linear refractive index, η is the coupling efficiency of the pump to the ring, P_{in} is the on-chip power of the pump and V is the mode volume of the microring resonator.

The instantiation of optical isolation within microring resonators is entirely predicated on the non-reciprocal nature of the Kerr effect, thereby obviating the necessity for any supplementary driving input. This design solely relies on a certain intensity of forward incident light, originating from the laser, and does not require any external electric or magnetic fields, making it a passive isolator. This optical isolator, which is predicated solely on the microring resonator, is congruent with the majority of ultra-low-loss thin-film lithium niobate fabrication processes. The insertion loss of this system hinges exclusively on the coupling coefficient that mediates the interaction between the ring and the waveguides. By meticulously adjusting the separation between them, it is feasible to attain a minimal insertion loss. However, it is imperative to recognize that the optimization of the microring resonators' insertion loss, while enhancing transmission, may inadvertently diminish the quality factor (Q). This reduction in Q can, in turn, lead to a decrement in isolation, thereby establishing a trade-off between the system's insertion loss and its isolation capability.

3. Results

Based on Eqs. (3) and (4), the attainment of high isolation in integrated photonics necessitates a platform that exhibits low loss, high power tolerance, pronounced third-order nonlinearity, and a compact mode volume. Lithium niobate, a material renowned for its exceptional properties, satisfies these criteria, making it an ideal candidate for the development of high-quality passive optical isolators. There is an exigent demand for such isolators in the field of integrated photonics. In this work, we present a passive optical isolator harnessing the properties of thin-film lithium niobate, showcasing its effectiveness in enabling non-reciprocal light transmission without the need for external driving forces.

Our device fabrication initiates with an X-cut LN-on-insulator wafer procured from NANOLN, featuring a 600-nm-thick lithium niobate (LN) thin film atop a 3-micron-thick buried oxide layer, seated on a silicon substrate. Employing electron beam lithography, we meticulously defined the pattern, which was subsequently transferred to the lithium niobate film through argon ion physical etching. The etch depth into the LN is precisely 300 nm, preserving a 300-nm slab across the chip. The waveguide's top width is designed to be 1200 nm, with the sidewall angle optimized at 75°. A comprehensive view of the entire device is presented in Fig. 2(a), where we employ a fiber array to channel light into the chip via grating couplers, incurring a coupling loss of 8 dB. Within Fig. 2(a), we have designated the four grating couplers as 1, 2, 3, and 4. A robust forward pump light is directed through grating coupler 3 and subsequently retrieved from grating coupler

1, with the associated transmittance indicated as T_{13}. Conversely, a weaker backward signal is introduced via grating coupler 4 and extracted from grating coupler 2, with the corresponding transmittance denoted as T_{24}. Additionally, a directional coupler is integrated into the chip, designed to achieve a power ratio of direct pass to cross pass of 10:1. The radius of the microring resonator is 100 μm and we tested the transmission at the drop port with the loaded quality factor of 5×10^5 as shown in Fig. 2(b).

Figure 2(c) illustrates the experimental configuration employed for the characterization of the isolator integrated within lithium niobate thin films. A tunable laser source emitting at 1550 nm is directed into a 50:50 power beam splitter, thereby distributing the light into two distinct pathways. The pump light, which is of higher intensity relative to the signal light, is introduced directly into the chip via an erbium-doped fiber amplifier (EDFA) and propagates in the clockwise (CW) direction. Given the weaker nature of the signal light, it is modulated using an electro–optical modulator to precisely ascertain the signal light's intensity. Subsequently, the signal light, with an on-chip power of 5-mW post-amplification through the EDFA, is fed into the chip. The output signal light is then conveyed through a photodetector and its power is measured using a lock-in amplifier, ensuring accurate detection of the signal.

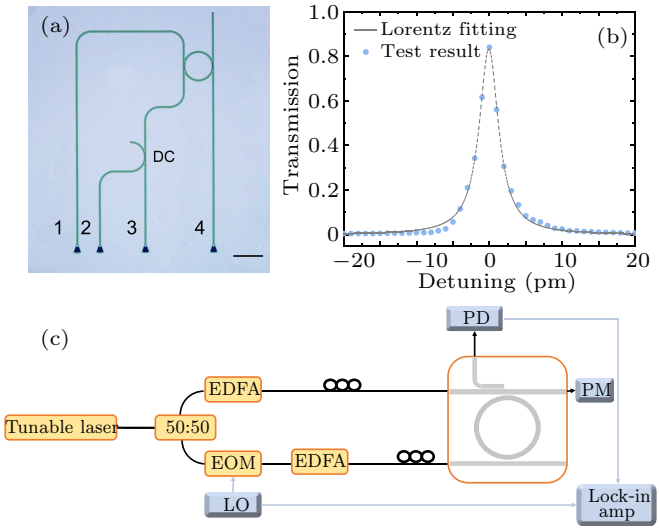

Fig. 2. (a) Image of a lithium niobate device. DC: directional coupler; scale bar: 200 μm; (b) transmission at the drop port; (c) the experimental setup for the characterization of an isolator in lithium niobate thin films. EDFA: erbium-doped fibre amplifier; PD: photodetector; EOM: electro–optical modulator; LO: 50-kHz electronic generator; Lock-in Amp: lock-in amplifier; PM: powermeter.

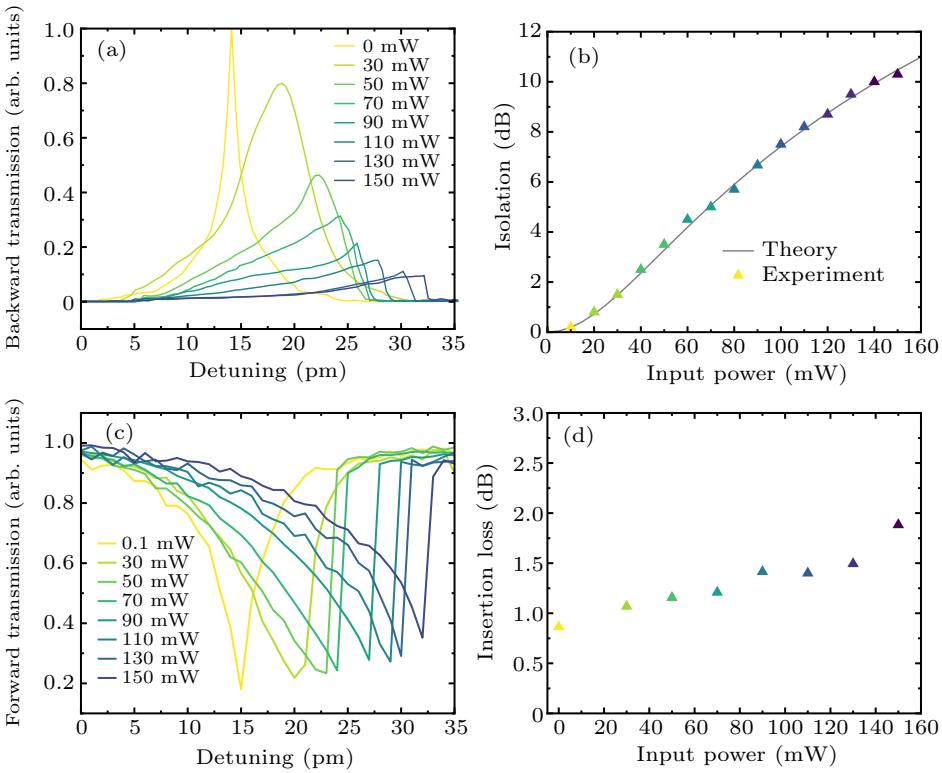

Fig. 3. (a) Backward light transmission under different forward light powers. (b) Theoretical and experimental device isolations. (c) Forward light transmission under different powers. (d) Insertion loss under different powers.

Figure 3(a) presents our methodology for scanning the transmission T_{24} of backward light at varying forward light powers, achieved by modulating the laser wavelength and the gain of the erbium-doped fiber amplifier (EDFA). During this scanning process, we discern that the resonance peak deviates from a Lorentzian profile at elevated power levels. This deviation arises from the thermal effect of the pump light, which induces a shift in the resonance of the microring resonator. As the laser frequency near the ring's resonance, an increasing amount of optical power is coupled into the resonant mode.

The linear absorption inherent in lithium niobate leads to the heating of the ring, causing the resonance to detune from the laser frequency. This results in a red-shift of the resonance frequency until the laser frequency aligns with the resonant frequency, at which point the coupling to the ring is maximized. Beyond this point of maximum coupling, as the laser detuning increases, the power within the ring diminishes, enabling the ring to cool and revert to its original resonant state. In Fig. 3(b), we illustrate the behavior of the backward light power transmitted through the ring, observing a gradual decrease as the forward light power increases. At a forward light power of 50 mW, the backward light power exhibits a 3-dB reduction. Upon further increasing the optical power to 150 mW, the attenuation of the backward light power can reach up to 10.3 dB. The demonstrated isolation of the signal under varying pump powers is found to be in excellent agreement with our theoretical predictions, thereby validating the effectiveness of our passive optical isolator design.

A pivotal parameter defining the performance of on-chip optical isolators is the insertion loss, which in the case of add-drop microring resonators, is predominantly governed by the coupling efficiency between the light and the ring. In our experiments, we scanned the transmission T_{13} of the pump light at varying power levels, with the outcomes delineated in Figs. 3(c) and 3(d). Our observations reveal that the insertion loss escalates incrementally with the augmentation of pump power. At a pump power of 0.1 mW, the insertion loss of the microring resonator is measured to be 0.91 dB, and this value rises to 1.87 dB at a pump power of 150 mW. The test outcomes indicate that while high-power forward light indeed leads to an elevation in insertion loss, this increase is nominal when juxtaposed with the substantial enhancement in isolation.

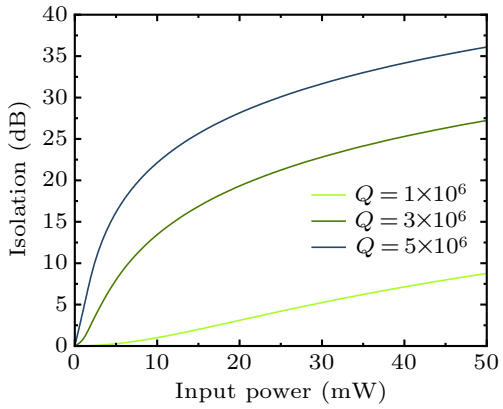

Fig. 4. Simulation results of isolation *versus* input power for different Q values. The simulation parameters for our device are as follows: an X-cut, 600-nm-thick TFLN with an etch depth of 350 nm and an angle of 60°. The top width of waveguide is 2.4 μm and is covered with a 1.5-μm-thick layer of SiO_2, serving as the upper cladding. The microring resonator, has a radius of 80 μm, and its coupling state is designed to achieve critical coupling.

4. Conclusion

We introduce a ground breaking, fully passive optical isolator fabricated from lithium niobate thin films. This device capitalizes on the modal splitting induced by the Kerr effect, which disrupts the reciprocity of the microring resonator and facilitates non-reciprocal light transmission. Our experimental demonstrations have achieved an isolation level exceeding 10 dB, with an insertion loss of merely 1.87 dB. The isolation performance of our device can be further optimized by elevating Q factor. State-of-the-art TFLN photonic chips can achieve Q factor more than 10^6, and in some instances, up to 10^8.[44–46] In Fig. 4, we present simulated results illustrating the variation of isolation with input power at different Q factors. The results demonstrate that at a Q factor of 5×10^6, an isolation of 20 dB is attainable with merely 8 mW of input power. This not only substantiates the feasibility of our design but also underscores the potential for significant enhancement in isolation efficiency through Q factor optimizations. Furthermore, the cascading of microring resonators presents an additional strategy for reducing the forward power required for effective isolation.[33]

The distinct advantage of our device lies in its complete passivity and lack of magnetic components, rendering it free from the need for external drivers. Moreover, this optical isolator eschews the need for complex fabrication processes, being realizable with the most rudimentary waveguide techniques. This simplicity substantially reduces the cost and integration complexity associated with optical isolators. The implications of such an isolator are profound, heralding a new era in the application of lithium niobate integrated photonic platforms. In addition, a high-quality factor microring resonator can perform self-injection locking on semiconductor laser chips while also providing isolation.[49] A device that integrates these dual functionalities is exceptionally well-suited for integration in chip-based applications. It is poised to significantly accelerate the development of on-chip integrated lasers, offering a robust solution for the next generation of photonic integrated circuits. The integration of this optical isolator within lithium niobate photonic circuits not only streamlines the construction of complex photonic devices but also enhances their performance by providing a reliable means of non-reciprocal light propagation. This innovation stands as a testament to the potential of lithium niobate as a material platform for the future of integrated photonics, paving the way for more sophisticated and versatile photonic systems.

Acknowledgement

Project supported by the National Key Research and Development Program of China (Grant Nos. 2022YFF0712800 and 2019YFA0308700).

References

[1] Shu H, Chang L, Tao Y, Shen B, Xie W, Jin, M, Netherton A, Tao Z, Zhang X, Chen R, Bai B, Qin J, Yu S, Wang X and Bowers J 2022 *Nature* **605** 457

[2] Lundberg L, Mazur M, Mirani A, Foo B, Schröder J, Torres-Company V, Karlsson M and Andrekson P 2020 *Nat. Commun.* **11** 201

[3] Marpaung D, Yao J and Capmany J 2019 *Nat. Photon.* **13** 80

[4] Sludds A, Bandyopadhyay S, Chen Z, Zhong Z, Cochrane J, Bernstein L, Bunandar D, Dixon P, Hamilton S, Streshinsky M, Novack A, Baehr-Jones T, Hochberg M, Ghobadi M, Hamerly R and Englund A 2022 *Science* **378** 270

[5] Xu X, Tan M, Corcoran B, Wu J, Boes A, Nguyen T, Chu S, Little B, Hicks D, Morandotti R, Mitchell A and Moss D 2021 *Nature* **589** 44

[6] Newman Z, Maurice V, Drake T, Stone J, Briles T, Spencer D, Fredrick C, Li Q, Westly D and Ilic B 2019 *Optica* **6** 680

[7] Wang J, Sciarrino F, Laing A and Thompson M 2020 *Nat. Photon.* **14** 273

[8] Zhao J, Ma C, Rüsing M and Mookherjea S 2020 *Phys. Rev. Lett.* **124** 163603

[9] Xin C, Mishra J, Chen C, Zhu D, Shams-Ansari A, Langrock C, Sinclair N, Wong N, Fejer M and Lončar M 2022 *Opt. Lett.* **47** 2830

[10] Kim I, Martins R, Jang J, Badloe T, Khadir S, Jung H, Kim H, Kim J, Genevet P and Rho J 2021 *Nat. Nanotechnol.* **16** 508

[11] Trocha P, Karpov M, Ganin D, Pfeiffer M, Kordts A, Wolf S, Krockenberger J, Marin-Palomo P, Weimann C, Randel S, Freude W, Kippenberg T and Koos C 2018 *Science* **359** 887

[12] Poulton C, Yaacobi A, Cole D, Byrd M, Raval M, Vermeulen D and Watts M 2017 *Opt. Lett.* **42** 4091

[13] Estevez M, Alvarez M and Lechuga L 2012 *Laser Photon. Rev.* **6** 463

[14] Shams-Ansari A, Yu M, Chen Z, Reimer C, Zhang M, Picqué N and Lončar M 2022 *Commun. Phys.* **5** 88

[15] Suh M, Yang Q, Yang K, Yi X and Vahala K 2016 *Science* **354** 600

[16] Jin W, Yang Q, Chang L, Shen B, Wang H, Leal M, Wu L, Gao M, Feshali A, Paniccia M, Vahala J K and Bower E J 2021 *Nat. Photon.* **15** 346

[17] Yan W, Yang Y, Liu S, Zhang Y, Xia S, Kang T, Yang W, Qin J, Deng L and Bi L 2020 *Optica* **7** 1555

[18] Huang D, Pintus P, Zhang C, Shoji Y, Mizumoto T and Bowers J 2016 *IEEE Journal of Selected Topics in Quantum Electronics* **22** 271

[19] Pintus P, Huang D, Zhang C, Shoji Y, Mizumoto T and Bowers J 2017 *J. Lightwave Technol.* **35** 1429

[20] Zhang Y, Du Q, Wang C, Fakhrul T, Liu S, Deng L, Huang D, Pintus P, Bowers J, Ross C, Hu J and Bi L 2019 *Optica* **6** 473

[21] Bi L, Hu J, Jiang P, Kim D, Dionne G, Kimerling L and Ross C 2011 *Nat. Photon.* **5** 758

[22] Lira H, Yu Z, Fan S and Lipson M 2012 *Phys. Rev. Lett.* **109** 033901

[23] Tzuang L, Fang K, Nussenzveig P, Fan S and Lipson M 2014 *Nat. Photon.* **8** 701

[24] Dostart N, Gevorgyan H, Onural D and Popović M 2021 *Opt. Lett.* **46** 460

[25] Bhandare S, Ibrahim S, Sandel D, Zhang H, Wust F and Noé R 2005 *IEEE Journal of Selected Topics in Quantum Electronics* **11** 417

[26] Doerr C, Dupuis N and Zhang L 2011 *Opt. Lett.* **36** 4293

[27] Doerr C, Chen L and Vermeulen D 2014 *Opt. Express* **22** 4493

[28] Herrmann J, Ansari V, Wang J, Witmer J, Fan S and Safavi-Naeini A 2022 *Nat. Photon.* **16** 603

[29] Yu M, Cheng R, Reimer C, He L, Luke K, Puma E, Shao L, Shams-Ansari A, Ren X, Grant H, Johansson L, Zhang M and Lončar M 2023 *Nat. Photon.* **17** 666

[30] Tian H, Liu J, Siddharth A, Wang R, Blésin T, He J, Kippenberg T and Bhave S 2021 *Nat. Photon.* **15** 828

[31] Sohn D, Örsel O and Bahl G 2021 *Nat. Photon.* **15** 822

[32] Kittlaus E, Jones W, Rakich P, Otterstrom N, Muller R and Rais-Zadeh M 2021 *Nat. Photon.* **15** 43

[33] White A, Ahn G, Gasse K, Yang K, Chang L, Bowers J and Vučković J 2023 *Nat. Photon.* **17** 143

[34] Del L, Silver J, Woodley M, Stebbings S, Zhao X and Del'Haye P 2018 *Optica* **5** 279

[35] Saha K, Okawachi Y, Kuzucu O, Menard M, Lipson M and Gaeta A 2013 *CLEO: OSA Technical Digest (online) (Optica Publishing Group)* QF1D–2

[36] Abdelsalam K, Li T, Khurgin J and Fathpour S 2020 *Optica* **7** 209

[37] Kitching J 2018 *Appl. Phys. Rev.* **5** 031302

[38] Yang K, Skarda J, Cotrufo M, Dutt A, Ahn H, Sawaby M, Vercruysse D, Arbabian A, Fan S, Alù A and Vučković J 2020 *Nat. Photon.* **14** 369

[39] Xuan Y, Liu Y, Varghese L, Metcalf A, Xue X, Wang P, Han K, Jaramillo-Villegas A, Al A, Wang C, Kim S, Teng M, Lee Y, Niu B, Fan L, Wang J, Leaird D, Weiner A and Qi M 2016 *Optica* **3** 1171

[40] Lu X, Lee J, Rogers S and Lin Q 2014 *Opt. Express* **22** 30826

[41] Wilson D, Schneider K, Hönl S, Anderson M, Baumgartner Y, Czornomaz L, Kippenberg T and Seidler P 2020 *Nat. Photon.* **14** 57

[42] Wang C, Zhang M, Yu M, Zhu R, Hu H and Loncar M 2019 *Nat. Commun.* **10** 978

[43] Yang F, Fang X, Chen X, Zhu L, Zhang F, Chen Z and Li Y 2022 *Chin. Opt. Lett.* **20** 022502

[44] Del L, Silver J, Stebbings S and Del'Haye P 2017 *Sci. Rep.* **7** 43142

[45] Zhang M, Wang C, Cheng R, Shams-Ansari A and Lončar M 2017 *Optica* **4** 1536

[46] Shams-Ansari A, Huang G, He L, Li Z, Holzgrafe J, Jankowski M, Churaev M, Kharel P, Cheng R, Zhu D, Sinclair N, Desiatov B, Zhang M, Kippenberg T and Lončar M 2022 *Appl. Photon.* **7** 081301

[47] Gao R, Yao N, Guan J, Deng L, Lin J, Wang M, Qiao L, Fang W and Cheng Y 2022 *Chin. Opt. Lett.* **20** 011902

[48] Zhuang R, He J, Qi Y and Li Y 2023 *Adv. Mater.* **35** 2370015

[49] White A D, Ahn G H, Luhtaru R, Guo J, Morin T J, Saxena A, Chang L, Majumdar A, Gasse K V, Bowers J E and Vučković J 2024 *Nat. Photon.* **18** 1305